

ALMA observations of N83C in the early stage of star formation in the Small Magellanic Cloud

Kazuyuki Muraoka¹, Aya Homma¹, Toshikazu Onishi¹, Kazuki Tokuda^{1,2}, Ryohei Harada¹, Yuuki Morioka¹, Sarolta Zahorecz^{1,2}, Kazuya Saigo², Akiko Kawamura², Norikazu Mizuno^{2,3}, Tetsuhiro Minamidani^{3,4}, Erik Muller², Yasuo Fukui⁵, Margaret Meixner^{6,7}, Remy Indebetouw^{8,9}, Marta Sewilo¹⁰

and

Alberto Bolatto¹¹

ABSTRACT

We have performed Atacama Large Millimeter/submillimeter Array (ALMA) observations in $^{12}\text{CO}(J=2-1)$, $^{13}\text{CO}(J=2-1)$, $\text{C}^{18}\text{O}(J=2-1)$, $^{12}\text{CO}(J=3-2)$, $^{13}\text{CO}(J=3-2)$, and $\text{CS}(J=7-6)$ lines toward the active star-forming region N83C in the Small Magellanic Cloud (SMC), whose metallicity is about one-fifth of the Milky Way (MW). The ALMA observations first reveal subparsec-scale molecular structures in $^{12}\text{CO}(J=2-1)$ and $^{13}\text{CO}(J=2-1)$ emissions. We found strong CO peaks associated with young stellar objects (YSOs) identified by the *Spitzer Space Telescope*, and we also found that overall molecular gas is distributed along the edge of the neighboring H II region. We derived a gas density of $\sim 10^4 \text{ cm}^{-3}$ in molecular clouds associated with YSOs based on the virial mass estimated from the $^{12}\text{CO}(J=2-1)$ emission. This high gas density is presumably due to the effect of the H II region under the low-metallicity (and accordingly small-dust content) environment in the SMC; far-UV radiation from the H II region can easily penetrate and photodissociate the outer layer of ^{12}CO molecules

¹Department of Physical Science, Graduate School of Science, Osaka Prefecture University, 1-1 Gakuen-cho, Naka-ku, Sakai, Osaka 599-8531, Japan

²Chile Observatory, National Astronomical Observatory of Japan, National Institutes of Natural Science, 2-21-1 Osawa, Mitaka, Tokyo 181-8588, Japan

³Department of Astronomical Science, School of Physical Science, SOKENDAI (The Graduate University of Advanced Studies), 2-21-1 Osawa, Mitaka, Tokyo 181-8588, Japan

⁴Nobeyama Radio Observatory, National Astronomical Observatory of Japan, National Institutes of Natural Science, 462-2 Nobeyama, Minamimaki-mura, Minamisaku-gun, Nagano 384-1305, Japan

⁵Department of Astrophysics, Nagoya University, Chikusa-ku, Nagoya 464-8602, Japan

⁶The Johns Hopkins University, Department of Physics and Astronomy, 366 Bloomberg Center, 3400 N. Charles Street, Baltimore, MD 21218, USA

⁷Space Telescope Science Institute, 3700 San Martin Drive, Baltimore, MD 21218, USA

⁸Department of Astronomy, University of Virginia, P.O. Box 400325, Charlottesville, VA 22904, USA

⁹National Radio Astronomy Observatory, 520 Edgemont Road, Charlottesville, VA 22903, USA

¹⁰NASA Goddard Space Flight Center, 8800 Greenbelt Road, Greenbelt, MD 20771, USA

¹¹Department of Astronomy, University of Maryland, College Park, MD 20742, USA

in the molecular clouds, and thus only the innermost parts of the molecular clouds are observed even in ^{12}CO emission. We obtained the CO-to- H_2 conversion factor X_{CO} of $7.5 \times 10^{20} \text{ cm}^{-2} (\text{K km s}^{-1})^{-1}$ in N83C based on virial masses and CO luminosities, and it is four times larger than that in the MW, $2 \times 10^{20} \text{ cm}^{-2} (\text{K km s}^{-1})^{-1}$. We also discuss the difference in the nature between two high-mass YSOs, each of which is associated with a molecular clump with a mass of about a few $\times 10^3 M_{\odot}$.

Subject headings: ISM: clouds — ISM: molecules — stars: formation

1. Introduction

Metallicity in the interstellar medium is one of the key parameters to control star-formation processes and molecular gas properties. In particular, an environment with low metallicity (and accordingly small-dust content) is important because it causes a reduction of the shielding against far-UV radiation from massive stars, which affects the formation, structure, and physical properties of giant molecular clouds (GMCs) as well as the star-formation process.

The Small Magellanic Cloud (SMC), which is classified as a dwarf irregular galaxy, is an ideal target to investigate molecular gas structures and star-formation processes under an environment with low metallicity and small-dust content because its metallicity is about one-fifth of the Sun (Dufour 1984; Kurt et al. 1999; Pagel 2003) and the dust-to-gas ratio is 17 times smaller than that in the Milky Way (MW; Koornneef (1984). In addition, its proximity (~ 60 kpc; Hilditch et al. 2005) enables us to perform high-spatial-resolution observations even at millimeter to submillimeter wavelengths.

Molecular clouds in the SMC have been observed in the $^{12}\text{CO}(J = 1 - 0)$, $^{13}\text{CO}(J = 1 - 0)$, $^{12}\text{CO}(J = 2 - 1)$, and $^{13}\text{CO}(J = 2 - 1)$ lines using the Swedish-ESO Submillimeter Telescope at angular resolutions of $45''$ (~ 13 pc) for $\text{CO}(J = 1 - 0)$ and $23''$ (~ 7 pc) for $\text{CO}(J = 2 - 1)$, and intensity ratios among these molecular lines have been examined by many authors (e.g., Israel et al. 1993; Rubio et al. 1993; Lequeux et al. 1994; Rubio et al. 1996; Israel et al. 2003). In addition, Mizuno et al. (2001) observed the SMC in the $^{12}\text{CO}(J = 1 - 0)$ line at an angular resolution of $2.6''$ using the NANTEN telescope, and they identified 21 GMCs whose masses are $\sim 10^4$ to $10^6 M_{\odot}$. They found a good spatial correlation between the GMCs and H II regions or young clusters, indicating that cluster formation is ongoing in these GMCs.

Here, we focus on the N83 region, which is located in the southeast wing of the SMC and is an isolated, yet relatively active star-forming region. The H II region contains the stellar association NGC456 and a possible supernova remnant (Haberl et al. 2000). Molecular gas delineates the edge of the H II region (Bolatto et al. 2003), and this indicates that the molecular cloud may be formed or compressed by the expanding shell. In addition, warm (~ 40 K) molecular gas exists in N83 that might be heated by the neighboring H II region (Bolatto et al. 2003; Bolatto et al. 2005). The CO-to- H_2 conversion factor (X_{CO}) in N83 was estimated to be $(7.0 \pm 3.4) \times 10^{20} \text{ cm}^{-2} (\text{K km s}^{-1})^{-1}$ (Bolatto et al. 2003).

In particular, Bolatto et al. (2003) found that the south clump N83C shows the most intense $\text{CO}(J = 2 - 1)$ emission in the N83 region, and its X_{CO} is lower than that in other regions of N83. They argued that X_{CO} decreases and reaches nearly Galactic values in CO-bright regions such as N83C (see also Glover & Clark 2012). However, these observations could not fully resolve molecular clouds (e.g., Israel et al. 2003), and thus smaller structures such as cores and filaments may exist. For such unresolved clouds, one cannot reveal the detailed evolutionary processes of molecular clouds associated with young stellar objects (YSOs). In

addition, the estimated X_{CO} might be uncertain, due to the uncertainties of the cloud geometry and the resultant virial mass. In order to resolve smaller molecular structures and to obtain more accurate X_{CO} values in the SMC, further observations with higher angular resolution are indispensable.

In this paper, we present the results of Atacama Large Millimeter/submillimeter Array (ALMA) observations toward N83C. Firstly, we reveal the distribution of molecular gas associated with YSOs based on the high-angular-resolution maps with ALMA. Then, we derive various properties of molecular clouds: virial mass, average gas density, kinetic temperature, and X_{CO} . Finally, we comprehensively discuss molecular gas properties and their relation to star formation in N83C.

2. Observations

ALMA Cycle 2 observations toward N83C were carried out in Band 6 (211 – 275 GHz) and Band 7 (275 – 373 GHz) with the main array 12 m antennas, the Atacama Compact Array (ACA) 7 m antennas, and total power (TP) 12 m antennas between 2014 May and 2015 September.

The observations were centered on $(\alpha_{\text{J2000}}, \delta_{\text{J2000}}) = (01^{\text{h}}14^{\text{m}}05^{\text{s}}.414, -73^{\circ}17'03''.908)$. The target molecular lines are $^{12}\text{CO}(J = 2 - 1)$, $^{13}\text{CO}(J = 2 - 1)$, and $\text{C}^{18}\text{O}(J = 2 - 1)$ in Band 6, and $^{12}\text{CO}(J = 3 - 2)$, $^{13}\text{CO}(J = 3 - 2)$, and $\text{CS}(J = 7 - 6)$ in Band 7 with a bandwidth of 117.19 MHz ($30.5 \text{ kHz} \times 3840 \text{ channels}$). Note that we used a spectral window for the observations of the continuum emission with a bandwidth of 1875.0 MHz ($488.3 \text{ kHz} \times 3840 \text{ channels}$) in Band 6. The maximum baseline of the 12 m array is 348.5 m and that of ACA is 48.9 m.

The data were reduced using the Common Astronomy Software Application (CASA) package. We applied natural weighting for both Band 6 and Band 7 data, which provided synthesized beam sizes of $1''.72 \times 1''.37$ ($0.50 \text{ pc} \times 0.40 \text{ pc}$ at 60 kpc) and $4''.64 \times 4''.33$ ($1.35 \text{ pc} \times 1.23 \text{ pc}$), respectively. Note that we only used ACA and TP data in Band 7 because we could not obtain the main-array data, and thus its beam size is larger than that in Band 6. The rms noise levels of molecular lines at the velocity resolution of 0.2 km s^{-1} are 17 mJy beam^{-1} in Band 6 and $148 \text{ mJy beam}^{-1}$ in Band 7, respectively.

3. Results and Analyses

3.1. Maps

Figures 1(a) and (b) show integrated intensity maps in $^{12}\text{CO}(J = 2 - 1)$ and $^{13}\text{CO}(J = 2 - 1)$ emission of N83C. The global distribution of $^{12}\text{CO}(J = 2 - 1)$ emission is quite similar to that of $^{13}\text{CO}(J = 2 - 1)$ emission. Strong peaks of CO emission correspond to the position of bright YSOs¹ (A and B), identified based on the *Spitzer Space Telescope* data (see also Figure 1(c)). Thus these YSOs are born within such CO-bright molecular clouds. We can see faint local peaks at sources C and D, but no CO emission is found at the source E. Figure 1(d) shows that local peaks of $\text{H}\alpha$ emission are associated with all of the sources, A to E. This implies that all of the YSOs are beginning to ionize the surrounding molecular gas. Overall molecular gas is distributed along the edge of the H II region.

¹We assigned the source ID to each YSO in alphabetical order according to the $^{12}\text{CO}(J = 2 - 1)$ peak temperature (see Table 1).

In Figures 2(a) and (b), we found a similar trend in the $J = 3 - 2$ transition as in the $J = 2 - 1$ transition (Figures 1(a) and (b)); that is, the global distributions of $^{12}\text{CO}(J = 3 - 2)$ and $^{13}\text{CO}(J = 3 - 2)$ are quite similar to each other, and strong peaks are observed at sources A and B in both CO emissions. Figures 2(c) and (d) show integrated intensity maps in the $\text{CS}(J = 7 - 6)$ and $\text{C}^{18}\text{O}(J = 2 - 1)^2$ emission of N83C. Although both lines can trace dense cores in molecular clouds, we find different features in their respective maps. The $\text{CS}(J = 7 - 6)$ intensity is stronger in source A than in source B, whereas the $\text{C}^{18}\text{O}(J = 2 - 1)$ peak is only observed at source B (see Section 4.2 in detail). The peak temperatures of each emission in sources A to E are summarized in Table 1.

We estimate the virial mass (M_{vir}) of molecular clouds associated with sources A and B as follows (Solomon et al. 1987):

$$M_{\text{vir}} = 1040\sigma_v^2 R, \quad (1)$$

where R is the radius of a molecular cloud in pc, and σ_v is the cloud velocity dispersion in km s^{-1} . Here, R was determined as the effective radius of the area whose CO intensity exceeds half the peak, and σ_v was calculated from the gaussian fitting of the CO line integrated over the area. Both R and σ_v are determined from the $^{12}\text{CO}(J = 2 - 1)$ map and the $^{13}\text{CO}(J = 2 - 1)$ map individually, as shown in Table 2. The resultant M_{vir} values are $\sim 10^3 M_{\odot}$.

Using the M_{vir} , we derive the average gas density $n(\text{H}_2)$ in the molecular clumps as follows:

$$n(\text{H}_2) = \frac{M_{\text{vir}}/(\mu_{\text{H}_2} \times m_{\text{H}})}{4\pi R^3/3}, \quad (2)$$

where $\mu_{\text{H}_2} \sim 2.7$ is the mean molecular weight per H_2 molecule (including the contribution by He), and m_{H} is the atomic hydrogen mass. The estimated $n(\text{H}_2)$ values are $\sim 10^4 \text{ cm}^{-3}$ (see Table 2).

3.2. Deriving gas density and kinetic temperature of molecular clouds

Here, we estimate gas density and kinetic temperature of molecular clouds using line ratios obtained from ALMA observations based on the Large Velocity Gradient (LVG) approximation (e.g., Goldreich & Kwan 1974; Scoville & Solomon 1974).

Firstly, we examined spatial distributions of $^{13}\text{CO}(J = 3 - 2)/^{12}\text{CO}(J = 3 - 2)$ and $^{13}\text{CO}(J = 3 - 2)/^{13}\text{CO}(J = 2 - 1)$ ratios as shown in Figures 3(a) and (b). We found local peaks corresponding to sources A and B in the $^{13}\text{CO}(J = 3 - 2)/^{12}\text{CO}(J = 3 - 2)$ ratio map, whereas such local peaks are not observed in the $^{13}\text{CO}(J = 3 - 2)/^{13}\text{CO}(J = 2 - 1)$ ratio map.

Then, we carried out the LVG calculation assuming the following input parameters: the molecular abundance $Z(^{12}\text{CO}) = [^{12}\text{CO}]/[\text{H}_2]$ of 8.0×10^{-6} , the $[^{12}\text{CO}]/[^{13}\text{CO}]$ abundance ratio of 50, and the velocity gradient dv/dr of $2.0 \text{ km s}^{-1} \text{ pc}^{-1}$. The assumed $Z(^{12}\text{CO})$ is based on that in the Large Magellanic Cloud (LMC); Mizuno et al. (2010) assumed $Z(^{12}\text{CO})$ of 1.6×10^{-5} in the LMC, whose metallicity is twice that in the SMC. Thus we assumed the twice smaller $Z(^{12}\text{CO})$ of 8.0×10^{-6} . The assumed $[^{12}\text{CO}]/[^{13}\text{CO}]$ of 50 is

²We used only ACA and TP data but excluded main-array data for $\text{C}^{18}\text{O}(J = 2 - 1)$ emissions because the main-array data degrade the resultant signal-to-noise ratio of the $\text{C}^{18}\text{O}(J = 2 - 1)$ map. Therefore, its beam size ($8''.25 \times 6''.06$) is larger than that of the $^{12}\text{CO}(J = 2 - 1)$ map ($1''.72 \times 1''.37$).

the same as that in the LMC (Mizuno et al. 2010). The assumed dv/dr of $2.0 \text{ km s}^{-1} \text{ pc}^{-1}$ is based on the size and the velocity dispersion of the molecular clump in source A (see Table 2).

Figures 3(c) and (d) show spatial distributions of molecular gas density and kinetic temperature, respectively. We found gas densities of $\sim 1.5 \times 10^4 \text{ cm}^{-3}$ and kinetic temperatures of $30 - 50 \text{ K}$ at sources A and B. The derived gas density based on the LVG calculation is consistent with that calculated from the virial mass. This implies that each molecular clump is gravitationally bounded. Note that we found a linear feature of high T_K ($\sim 90 \text{ K}$) from southeast to northwest in Figure 3(d). This is due to the breakdown of the one-zone model in the LVG approximation by the overlap of molecular gas with multiple velocity components.

4. Discussion

4.1. X_{CO} in the SMC

So far, X_{CO} in molecular clouds has been estimated mainly using virial masses and CO luminosities. It is reported that the standard X_{CO} value in the MW disk is $2 \times 10^{20} \text{ cm}^{-2} (\text{K km s}^{-1})^{-1}$ (Bolatto et al. 2013 and references therein). However, X_{CO} may vary depending on the mass and the definition of molecular clouds; for example, smaller clouds tend to have higher X_{CO} , i.e., $X_{\text{CO}} \propto L_{\text{CO}}^{-0.2}$ (Bolatto et al. 2013). Our ALMA observations spatially resolved molecular clumps associated with YSOs (sources A and B); each clump is an active site of star formation and is likely to have nearly a round shape. This indicates that each clump is likely to be gravitationally bounded, which is also estimated from the LVG analysis in Section 3.2, with nearly a spherical shape. Thus we derive the “spatially-resolved” X_{CO} of sources A and B in N83C and compare it with that obtained in earlier studies for SMC and the MW. The X_{CO} value can be calculated from the following equation:

$$X_{\text{CO}} = \frac{M_{\text{vir}}/(\mu_{\text{H}_2} \times m_{\text{H}})}{L_{\text{CO}}}, \quad (3)$$

where L_{CO} is the $^{12}\text{CO}(J = 1 - 0)$ luminosity of the molecular cloud. In order to calculate L_{CO} from our $^{12}\text{CO}(J = 2 - 1)$ data, we assume the $^{12}\text{CO}(J = 2 - 1)/^{12}\text{CO}(J = 1 - 0)$ ratio of 0.9 according to Bolatto et al. (2003). This ratio of 0.9 is consistent with the massive star-forming region in the MW (e.g., Nishimura et al. 2015). For source A, M_{vir} of $2.5 \times 10^3 M_{\odot}$ and L_{CO} of $186 \text{ K km s}^{-1} \text{ pc}^2$ yield X_{CO} of $6.2 \times 10^{20} \text{ cm}^{-2} (\text{K km s}^{-1})^{-1}$. In addition, we obtained a similar X_{CO} from source B, $8.7 \times 10^{20} \text{ cm}^{-2} (\text{K km s}^{-1})^{-1}$, from M_{vir} of $1.5 \times 10^3 M_{\odot}$ and L_{CO} of $81 \text{ K km s}^{-1} \text{ pc}^2$. The averaged X_{CO} of $7.5 \times 10^{20} \text{ cm}^{-2} (\text{K km s}^{-1})^{-1}$ is four times higher than that in the MW disk, which is in good agreement with that in N83 obtained by Bolatto et al. (2003), $(7.0 \pm 3.4) \times 10^{20} \text{ cm}^{-2} (\text{K km s}^{-1})^{-1}$.

4.2. Properties of molecular gas and star formation in N83C

We summarize the properties of the molecular gas based on our ALMA observations and discuss their relation to star formation in N83C.

The derived gas density of $\sim 10^4 \text{ cm}^{-3}$ is significantly higher than the typical gas density of $2 \times 10^3 \text{ cm}^{-3}$ in the Orion A/B molecular clouds (Nishimura et al. 2015), even though both gas densities are derived from the same molecular line, $^{12}\text{CO}(J = 2 - 1)$. Such a difference in derived gas densities is presumably due to the low metallicity in the SMC. The low metallicity corresponds to the small-dust content in molecular clouds,

which causes the reduction of the shielding against far-UV radiation. In this condition, external far-UV radiation from the H II region associated with N83C easily penetrates and photodissociates the outer layer of the ^{12}CO molecule in the molecular clouds. Thus we can only observe the innermost parts of the molecular clouds, whose gas density is $\sim 10^4 \text{ cm}^{-3}$, even in ^{12}CO emission. It is to be noted that theoretical simulations examined by Glover & Clark (2012) support our results: their simulations suggest that diffuse CO emission becomes unobservable, but dense gas continues to produce observable CO emission as metallicity decreases. The observational fact that even ^{12}CO emission traces the high-density ($\sim 10^4 \text{ cm}^{-3}$) regions in N83C just corresponds to this situation.

Then, we consider the meaning of the derived kinetic temperature of molecular gas, 30 – 50 K. Bolatto et al. (2003) suggested that warm ($\sim 40 \text{ K}$) clumps exist in some regions of N83 whose $^{12}\text{CO}(J = 2 - 1)/^{12}\text{CO}(J = 1 - 0)$ ratios exceed 2. Although the $^{12}\text{CO}(J = 2 - 1)/^{12}\text{CO}(J = 1 - 0)$ ratio of 0.9 in N83C is not so high (Bolatto et al. 2003; Bolatto et al. 2005), it is possible that the global gas temperature exceeds 30 K in N83C considering that the bright H II region, which is a likely heating source, spreads over N83. In addition, the kinetic temperature of molecular gas is consistent with the dust temperature of 35 K (Takekoshi et al. 2017). Recent observational studies in the MW can also support our results: Nishimura et al. (2015) reported that the kinetic temperature in Orion A/B molecular clouds is 20 – 50 K, which is similar to that in the N83C, although the typical temperature of molecular clouds in the MW is 10 – 20 K. Considering that both N83C and Orion A/B molecular clouds are associated with bright H II regions, it is suggested that their temperature increase is due to the heating by far-UV radiation. However, Nishimura et al. (2015) also found a temperature gradient in Orion A/B molecular clouds; the kinetic temperature decreases with distance from the H II region, while such a temperature gradient extending over more than a few parsecs is not observed in N83C with the spatial resolution of $\sim 1 \text{ pc}$. Thus there is a possibility that the molecular gas temperature in N83C is intrinsically high before the generation of the neighboring H II region.

Finally, we discuss the difference in the nature between sources A and B. As described in Section 3.1, the $\text{CS}(J = 7 - 6)$ intensity is stronger in source A than in source B, whereas the $\text{C}^{18}\text{O}(J = 2 - 1)$ peak is only observed at source B. This can be explained by the effects of far-UV radiation from the internal YSOs. Strong far-UV radiation can photochemically enhance CS emission (e.g., Zhou et al. 1991; Jansen et al. 1994; Sternberg & Dalgarno 1995) but dissociate the C^{18}O molecules (e.g., Shimajiri et al. 2014). Considering the luminosity of source A, $20140 L_{\odot}$, is three times larger than that of source B, $6899 L_{\odot}$ (Kamath et al. 2014), our observational results suggest that strong far-UV radiation from bright YSOs enhances CS emission but dissociates C^{18}O molecule in source A, while such effects do not work in source B because of its lower brightness. However, we found an opposite trend in the distribution of $\text{H}\alpha$ flux. As shown in the left panel of Figure 4, the peak of $\text{H}\alpha$ emission is not observed at source A, where $\text{H}\alpha$ emission is weak, although the strong $\text{H}\alpha$ peak is observed at source B. In order to reveal the cause of the weak $\text{H}\alpha$ emission in source A, we examined the spatial comparison between $\text{H}\alpha$ flux and the Band 6 continuum emission, which corresponds to emission from cold dust, as shown in the right panel of Figure 4. The strongest peak of the Band 6 continuum emission is coincident with the position of source A, and a possible peak is found at source B. This implies a very high density (and presumably unresolved) gas clump at source A and there seems to be a deeply embedded and very cold YSO therein, although the molecular gas density estimated from the LVG calculation is similar between sources A and B ($1.5 \times 10^4 \text{ cm}^{-3}$). Note that the source A is seen at the *BVI* bands (Kamath et al. 2014) in spite of the existence of the high-density clump, indicating that source A is likely a composite with a YSO deeply embedded. We also note the $\text{H}\alpha$ peak located to the south of source A, which is labeled as source F in Figure 4. It seems that the *Spitzer* map cannot resolve sources A and F spatially, as shown in Figure 1(c). In addition, the CO clump at source A elongates toward source F. These

observational facts indicate that source F is also a YSO as are sources A to E.

5. Summary and Conclusions

We have performed ALMA Cycle 2 observations in the $^{12}\text{CO}(J = 2 - 1)$, $^{12}\text{CO}(J = 2 - 1)$, $\text{C}^{18}\text{O}(J = 2 - 1)$, $^{12}\text{CO}(J = 3 - 2)$, $^{13}\text{CO}(J = 3 - 2)$ and $\text{CS}(J = 7 - 6)$ lines toward N83C. We summarize this work as follows:

1. We have successfully obtained subparsec-scale molecular structures in $^{12}\text{CO}(J = 2 - 1)$ and $^{13}\text{CO}(J = 2 - 1)$ emissions, and we found strong CO peaks associated with YSOs. Overall molecular gas is distributed along the edge of the H II region.
2. We derived a gas density of $\sim 10^4 \text{ cm}^{-3}$ of molecular clouds associated with YSOs based on the virial mass estimated from $^{12}\text{CO}(J = 2 - 1)$ emission as well as the LVG calculation. Since the outer layer of ^{12}CO molecules in the molecular clouds might be photodissociated, we can only observe the innermost parts of the molecular clouds with high gas density.
3. We obtained X_{CO} of $7.5 \times 10^{20} \text{ cm}^{-2} (\text{K km s}^{-1})^{-1}$ for star-forming clumps in N83C based on virial masses and CO luminosities, a number that is four times larger than that in the MW, $2 \times 10^{20} \text{ cm}^{-2} (\text{K km s}^{-1})^{-1}$. Note that clouds with L_{CO} much smaller than $10^5 \text{ K km s}^{-1} \text{ pc}^2$ have X_{CO} a few times larger than this standard value, even in the MW (Bolatto et al. 2013).
4. We derived the kinetic temperature of the molecular clouds of 30 – 50 K. There are two possibilities to explain such a high temperature: one is the heating from the neighboring H II region, and the other is that the molecular gas temperature in N83C is intrinsically high before the generation of the neighboring H II region.
5. We discussed the difference in the nature between two high-mass YSOs, each of which is associated with a molecular clump with a mass of about a few $\times 10^3 M_{\odot}$. The luminosities of YSOs are brighter in source A than in source B, whereas H α emission is brighter in source B than in source A. Considering the strong peak of the Band 6 (230 GHz) continuum emission at source A, a very high-density gas clump may exist.

Table 1. Properties in Each Molecular Line

Molecular line	Peak Temperature in Each Source					Beam Size (arcsec)	Position Angle (degree)	Rms Noise Level	
	A	B	C	D	E			(mJy beam $^{-1}$)	(mK)
$^{12}\text{CO}(J=2-1)$	24.4	21.7	18.7	7.1	5.6	$1''.72 \times 1''.37$	44°	17	162
$^{13}\text{CO}(J=2-1)$	7.2	7.9	4.3	1.9	1.6	$1''.75 \times 1''.40$	46°	19	188
$^{12}\text{CO}(J=3-2)$	18.6	14.6	13.8	3.5	1.7	$4''.64 \times 4''.33$	-33°	148	68
$^{13}\text{CO}(J=3-2)$	4.1	4.2	2.8	0.52	0.37	$4''.93 \times 4''.62$	61°	174	79
$\text{CS}(J=7-6)$	0.58	0.49	0.36	$4''.75 \times 4''.06$	56°	113	64
$\text{C}^{18}\text{O}(J=2-1)$	0.077	0.10	0.079	$8''.25 \times 6''.06$	86°	37	16

References for YSOs: A and B are identified by Kamath et al. (2014), and C, D, and E are by Sewilo et al. (2013).

We thank the anonymous referee for helpful comments, which significantly improved the manuscript. This paper makes use of the following ALMA data: [ADS/JAO.ALMA#2013.1.00212.S]. ALMA is a partnership of ESO (representing its member states), NSF (USA) and NINS (Japan), together with NRC (Canada), NSC and ASIAA (Taiwan), and KASI (Republic of Korea), in cooperation with the Republic of Chile. The Joint ALMA Observatory is operated by ESO, AUI/NRAO and NAOJ. This work is based on observations made with the *Spitzer Space Telescope*, which is operated by the Jet Propulsion Laboratory, California Institute of Technology under a contract with NASA. This research made use of APLpy, an open-source plotting package for Python Robitaille & Bressert (2012). This work was supported by NAOJ ALMA Scientific Research Grant Number 2016-03B and JSPS KAKENHI (Grant Nos. 17K14251, 22244014, 23403001, and 26247026). This work was also supported by the Mitsubishi Foundation. M. Meixner was supported by NSF grant 1312902.

REFERENCES

- Bolatto, A. D., Israel, F. P., & Martin, C. L. 2005, *ApJ*, 633, 210
- Bolatto, A. D., Leroy, A., Israel, F. P., & Jackson, J. M. 2003, *ApJ*, 595, 167
- Bolatto, A. D., Wolfire, M., & Leroy, A. K. 2013, *ARA&A*, 51, 207
- Dufour, R. J. 1984, in *IAU Symp. 108, Structure and Evolution of the Magellanic Clouds*, ed. S. van den Bergh, & K. S. D. de Boer (Dordrecht: Reidel), 353
- Goldreich, P., & Kwan, J. 1974, *ApJ*, 189, 441
- Glover, S. C. O., & Clark, P. C. 2012, *MNRAS*, 426, 377
- Haberl, F., Filipović, M. D., Pietsch, W., & Kahabka, P. 2000, *A&AS*, 142, 41
- Hilditch, R. W., Howarth, I. D., & Harries, T. J. 2005, *MNRAS*, 357, 304
- Israel, F. P., Johansson, L. E. B., Lequeux, J., et al. 1993, *A&A*, 276, 25
- Israel, F. P., Johansson, L. E. B., Rubio, M., et al. 2003, *A&A*, 406, 817
- Jansen, D. J., van Dishoeck, E. F., & Black, J. H. 1994, *A&A*, 282, 605
- Kamath, D., Wood, P. R., & Van Winckel, H. 2014, *MNRAS*, 439, 2211

Source	molecular line	σ_v (km s ⁻¹)	R (pc)	M_{vir} (M_{\odot})	H ₂ density (cm ⁻³)	L_{CO} (K km s ⁻¹ pc ²)
A	¹² CO($J=2-1$)	1.69	0.8	2.5×10^3	1.5×10^4	186
	¹³ CO($J=2-1$)	1.33	0.7	1.4×10^3	1.2×10^4	...
B	¹² CO($J=2-1$)	1.60	0.6	1.5×10^3	2.8×10^4	81
	¹³ CO($J=2-1$)	0.94	0.6	5.8×10^2	7.9×10^3	...

L_{CO} means the CO($J = 1 - 0$) luminosity assuming the CO($J = 2 - 1$)/CO($J = 1 - 0$) intensity ratio of 0.9.

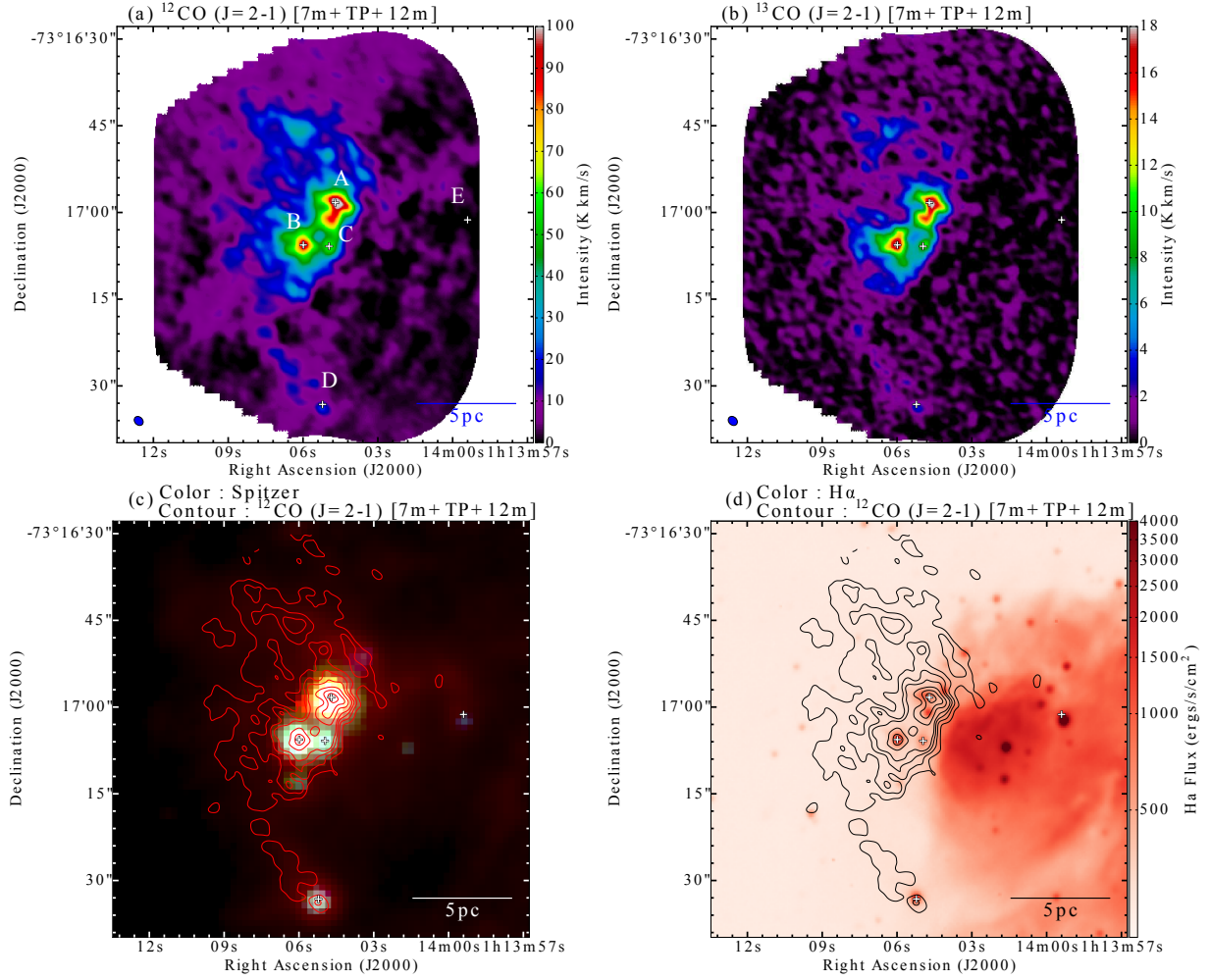


Fig. 1.— (a) Integrated intensity map in $^{12}\text{CO}(J = 2 - 1)$ emission of N83C. Crosses show the positions of bright sources (YSOs) identified by the *Spitzer Space Telescope* (Sewilo et al. 2013; Kamath et al. 2014). The synthesized beam is shown in the lower left corner. (b) Integrated intensity map in $^{13}\text{CO}(J = 2 - 1)$ emission. (c) Three-color composite *Spitzer*/IRAC image (blue: $3.6\ \mu\text{m}$, green: $4.5\ \mu\text{m}$, and red: $8\ \mu\text{m}$) superposed on the integrated intensity map in $^{12}\text{CO}(J = 2 - 1)$ emission (contour). The contour levels are 10, 20, 30, 40, 60, 80, and $100\ \text{K km s}^{-1}$. (d) $\text{H}\alpha$ flux map (color, Li et al. 2017) superposed on the integrated intensity map in $^{12}\text{CO}(J = 2 - 1)$ emission (contour). The contour levels are the same as in (c).

Kurt, C. M., Dufour, R. J., Garnett, D. R., et al. 1999, *ApJ*, 518, 246

Koornneef, J. 1984, in *IAU Symp. 108, Structure and Evolution of the Magellanic Clouds*, ed. S. van den Bergh, & K. S. D. de Boer (Dordrecht: Reidel), 333

Lequeux, J., Le Bourlot, J., Pineau des Forets, G., et al. 1994, *A&A*, 292, 371

Li, C.-J., Chu, Y.-H., Gruendl, R. A., et al. 2017, *ApJ*, 836, 85

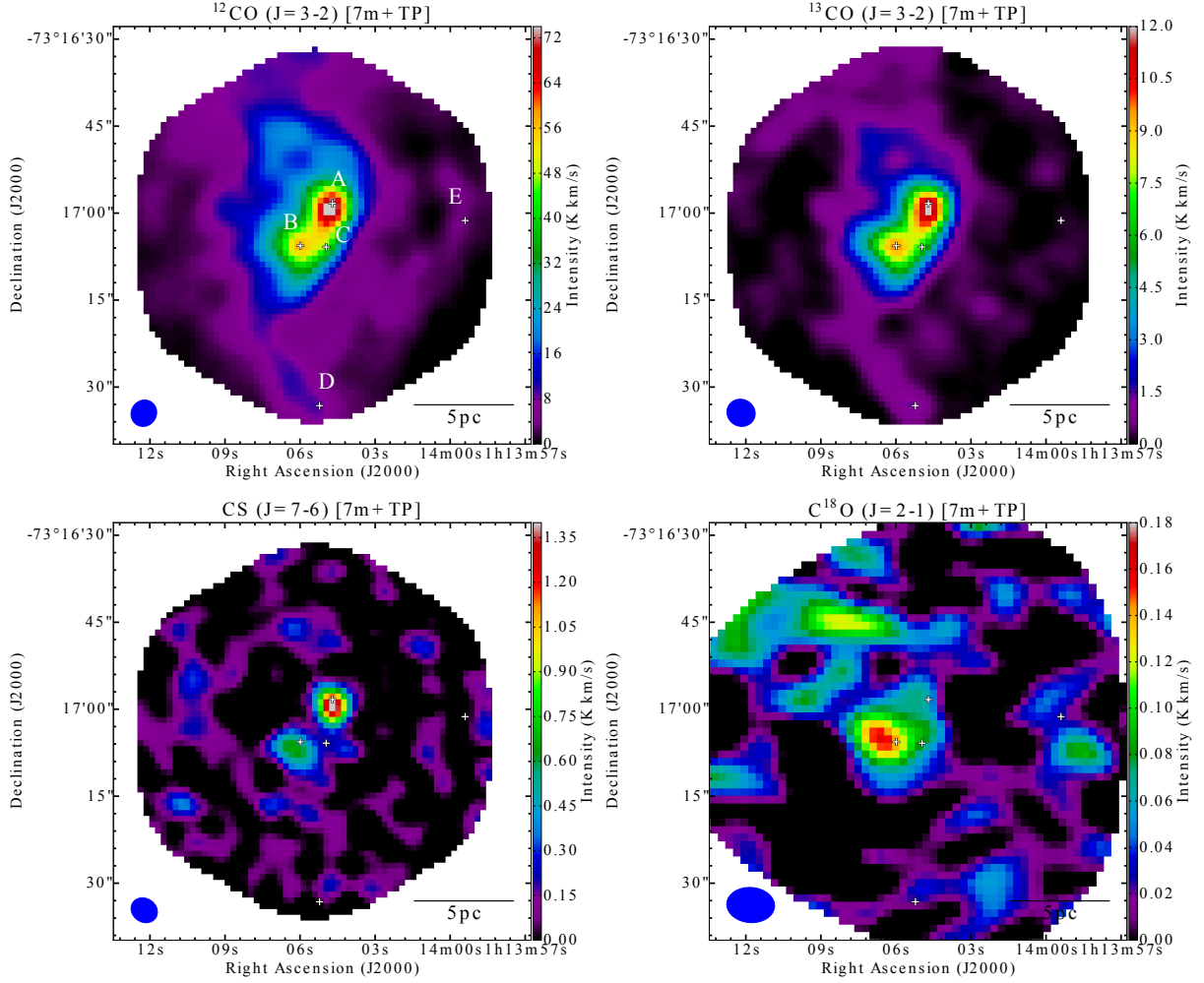


Fig. 2.— Integrated intensity maps in $^{12}\text{CO}(J = 3-2)$, $^{13}\text{CO}(J = 3-2)$, $\text{CS}(J = 7-6)$, and $\text{C}^{18}\text{O}(J = 2-1)$ emission of N83C. The synthesized beam is shown in the lower left corner of each map.

Mizuno, N., Rubio, M., Mizuno, A., et al. 2001, PASJ, 53, L45

Mizuno, Y., Kawamura, A., Onishi, T., et al. 2010, PASJ, 62, 51

Nishimura, A., Tokuda, K., Kimura, K., et al. 2015, ApJS, 216, 18

Pagel, B. E. J. 2003, in ASP Conf. Ser. 304, CNO Abundances in Dwarf and Spiral Galaxies, ed. C. Charbonnel, D. Schaerer & G. Meynet (San Francisco, CA: ASP), 187

Robitaille, T., & Bressert, E. 2012, APLpy: Astronomical Plotting Library in Python, Astrophysics Source Code Library, ascl:1208.017

Rubio, M., Lequeux, J., Boulanger, F., et al. 1993, A&A, 271, 1

Rubio, M., Lequeux, J., Boulanger, F., et al. 1996, A&AS, 118, 263

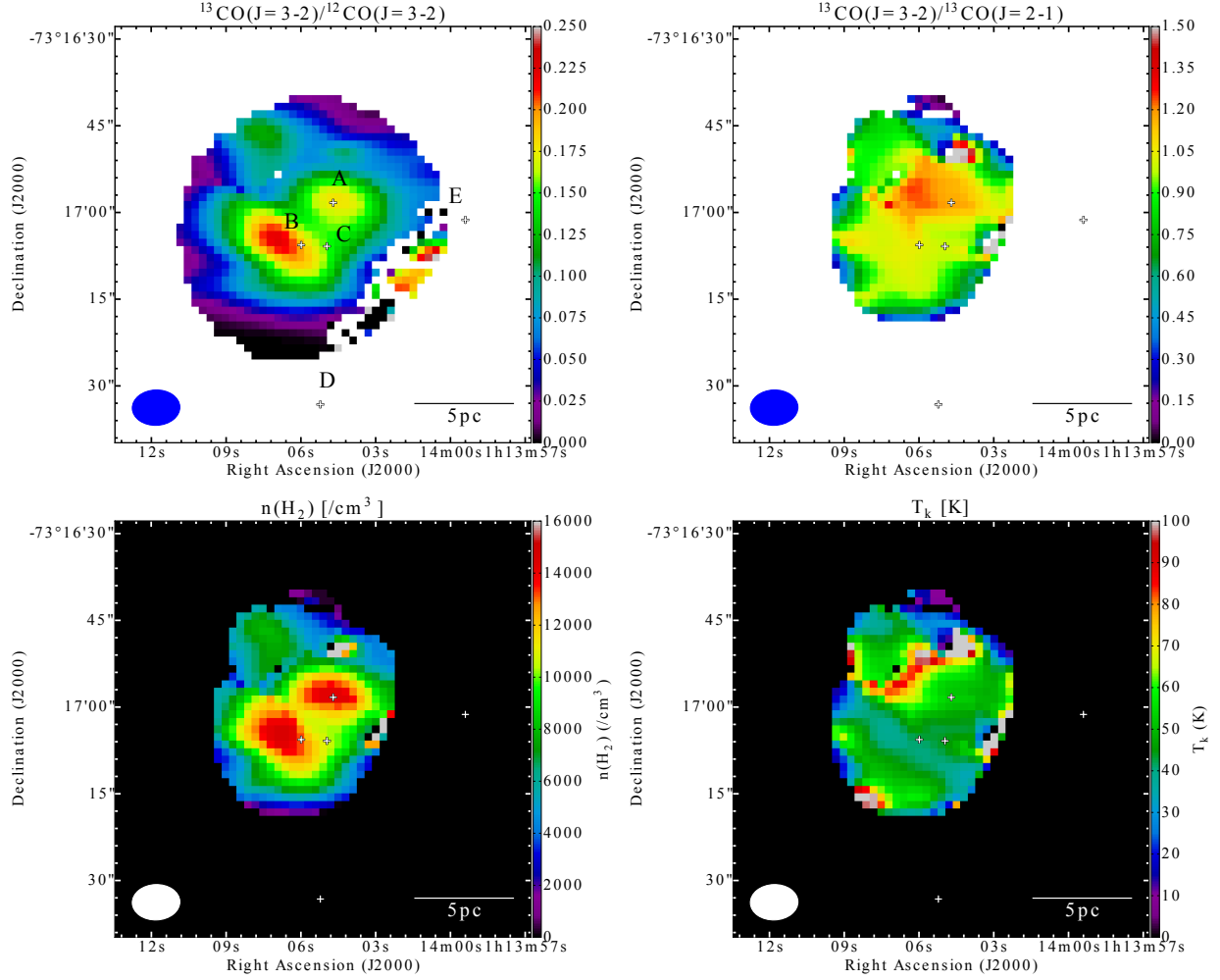


Fig. 3.— Top: spatial distributions of the $^{13}\text{CO}(J=3-2)/^{12}\text{CO}(J=3-2)$ and the $^{13}\text{CO}(J=3-2)/^{13}\text{CO}(J=2-1)$ intensity ratios of N83C. Bottom: spatial distributions of molecular gas density $n(\text{H}_2)$ and kinetic temperature T_k of N83C derived from the LVG calculation.

Scoville, N. Z. & Solomon, P. M. 1974, ApJ, 187, L67

Sewilo, M., Carlson, L. R., Seale, J. P., et al. 2013, ApJ, 778, 15

Shimajiri, Y., Kitamura, Y., Saito, M., et al. 2014, A&A, 564, A68

Solomon, P. M., Rivolo, A. R., Barrett, J., & Yahil, A. 1987, ApJ, 319, 730

Sternberg, A., & Dalgarno, A. 1995, ApJS, 99, 565

Takekoshi, T., Minamidani, T., Komugi, S., et al. 2017, ApJ, 835, 55

Zhou, S., Evans, N. J., II, Guesten, R., Mundy, L. G., & Kutner, M. L. 1991, ApJ, 372, 518

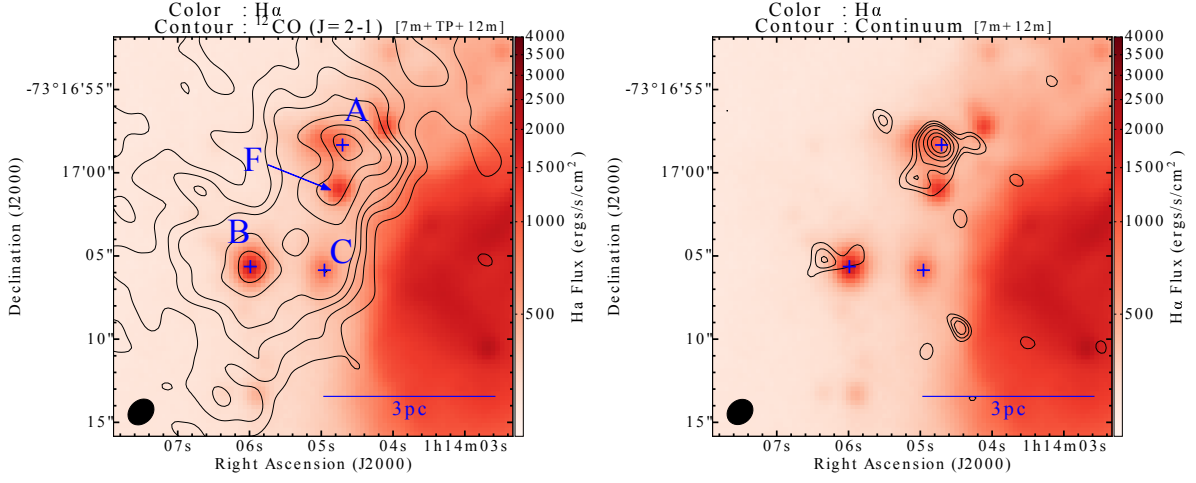


Fig. 4.— Left: enlarged view of Figure 1(d): integrated intensity map in $^{12}\text{CO}(J = 2 - 1)$ emission (contour) superposed on H α flux map (color) at sources A to C and F in N83C. The contour levels are the same as in Figure 1(d). Right: map of Band 6 continuum emission (contour) superposed on H α flux map (color) in N83C. The contour levels are 3, 4, 5, 7, 9, and 11 σ , where $1 \sigma = 0.2 \text{ mJy beam}^{-1}$. The synthesized beam is shown in the lower left corner.